Intercomparison of aerosol measurements performed with multi-wavelength Raman lidars, automatic lidars and ceilometers in the frame of INTERACT-II campaign

5 Fabio Madonna[1], Marco Rosoldi[1], Simone Lolli[1], Francesco Amato[1], Joshua Vande Hey[2], Ranvir Dhillon[2], Yunhui Zheng[3], Mike Brettle[4], Gelsomina Pappalardo[1].

[1]Istituto di Metodologie per l'Analisi Ambientale, Consiglio Nazionale delle Ricerche (CNR-IMAA)
[2]University of Leicester, Leicester, UK
10 [3]Sigma Space Corporation, Lanham, MD, US
[4]Campbell Scientific, Shepshed, UK

Correspondence to: Fabio Madonna (fabio.madonna@imaa.cnr.it)

15 **Abstract**. Following on from the previous efforts of INTERACT (INTERcomparison of Aerosol and Cloud Tracking), the INTERACT-II campaign used multi-wavelength Raman lidar measurements to assess the performance of an automatic compact micro-pulse lidar (MiniMPL) and two ceilometers (CL51 and CS135), respectively, to provide reliable information about optical and geometric atmospheric aerosol properties. The campaign took place at the CNR-IMAA Atmospheric Observatory (760 m asl, 40.60° N, 15.72° E), in the framework of the ACTRIS-2 (Aerosol Clouds Trace 20 gases Research InfraStructure) H2020 project. Co-located simultaneous measurements involving a MiniMPL, two ceilometers, and two EARLINET multi-wavelength Raman lidars (MUSA and PEARL) were performed from July to December 2016. Range-corrected signals (RCS) of MiniMPL showed an average difference with respect to MUSA/PEARL RCS of less than 10-15% below 3.0 km above sea level, largely due to the use of an inaccurate overlap correction, and smaller than 5 % in the free troposphere. For the CL51, the average difference with respect to 25 MUSA/PEARL attenuated backscatter is <20-30 % below 3 km, larger above. The variability of the CL51 calibration constant is within ±30 %. For the CS135, the performance is similar to the CL51 in the region below 2.0 km asl, while in the region above 3 km asl the differences are ±40 %. The variability of the CS135 normalization constant is within ±40-50 %.

Finally, following up to the outcome of a few specific tests performed during the campaign using the CHM15k ceilometer, 30 the CHM15k historical dataset available at CIAO from 2010 to 2016 were investigated to evaluate potential effect of the ceilometer laser fluctuations on calibration stability. The time series of the laser pulses shows an average variability of 10 % with respect to the nominal power which conforms to the specification. Nevertheless, laser pulses variability follows seasonal behavior with an increase in the number of laser pulses in summer and a decrease in winter. This may partly explain the dependency of the ceilometer calibration constant on the environmental temperature hypothesized during 35 INTERACT.

1. Introduction

The accurate monitoring of Essential Climate Variables (ECV) based on the use of low-cost and low-maintenance automatic system represents one of the challenges for the scientific community and instrument manufacturers for the next 40 decade. The use of automatic lidars for the profiling of the boundary layer and of aerosol properties in the free troposphere has reported continuous progress over the last years. Single wavelength elastic backscattering lidar, often with polarimetric capabilities, and ceilometers have the potential to improve our understanding of climate and air quality due to a dense deployment at the global scale (e.g. https://www.dwd.de/DWD/forschung/projekte/ceilomap/files/Legend_en.pdf). Advanced research lidars undoubtedly

45 are still the reference to monitor ECV but due to their complexity and high operation and maintenance costs have a limited geographical coverage. Even when federated networks have been set-up by international stakeholders (e.g. GALION – GAW Lidar Observation Network), the different practices adopted within each of the federated networks (e.g. EARLINET, MPLNET, ADNET, LALINET) significantly affect the homogeneity of the collected measurements; at present only one example of a coordinated monitoring of a global scale event (Nabro volcanic eruption) has been provided

50 in literature (Sawamura et al., 2011).

It is useful for the scientific community to understand to what extent automatic lidars and ceilometers (ALCs) are able to provide an estimation of the aerosol geometric and optical properties and fill in the geographical gaps of the existing advanced lidar networks, like EARLINET (European Aerosol Research Lidar NETwork, Pappalardo et al, 2014). In this direction, at European level, E-PROFILE (http://eumetnet.eu/activities/observations-programme/current-activities/e-

55 profile/), part of the EUMETNET Composite Observing System (EUCOS), along with EU COST-1303 TOPROF (http://www.toprof.imaa.cnr.it) is spending a large effort to characterize a few of the state-of-the-art ALCs and to establish a good understanding of the instrument output.

Limitations in aerosol property retrievals by different ceilometers have been already investigated (e.g. Wiegner et al. 2014, Madonna et al., 2015, Kotthaus et al., 2016). Ceilometers are limited to retrieving the attenuated backscatter and

60 the aerosol backscattering coefficient with a limited accuracy. For the latter, the retrieval is affected by the calibration of the aerosol backscattering profiles and relies on the use of ancillary instruments, such as a co-located Raman multi-wavelength lidar or a sun photometer, or, depending on the ceilometer model, can be performed using the molecular backscattering profile (only by adopting long integration time, larger than 1-2 hours depending on the atmospheric conditions (Wiegner et al., 2014). Alternatively, ceilometers can be calibrated scaling the backscatter signal until the

65 observed lidar ratio matches the theoretical value when suitable conditions of stratocumulus are available (O'Connor et al., 2004). In addition, ceilometers use diode laser sources working in an infrared region where the water vapor absorption is strong. At those wavelength regions, a correction of the profiles using a radiative transfer model is mandatory for retrieving optical properties (Wiegner and Gasteiger, 2015).

The INTERACT campaign took place at CIAO (CNR-IMAA Atmospheric Observatory) in Tito Scalo, Potenza, Italy

70 (760 m asl, 40.60°N, 15.72°E) from July 2014 to January 2015 (Madonna et al., 2015). It demonstrated good performance of the ceilometers using diode-pumped Nd:YAG lasers, like the CHM15k type, but also pointed out difficulties using the molecular calibration to retrieve aerosol properties. The variability of the ceilometer calibration constant, calculated using an advanced multi-wavelength Raman lidar as the reference, requires a frequent monitoring of the calibration at minimum on a seasonal basis. Thermal effects along with a non-linear system response to different aerosol loadings on the system

75 stability have been considered the potential reason for the Nd:YAG ceilometers' instability.

With the same general campaign objectives to INTERACT, i. e. to provide a continuous investigation of the automatic lidar and ceilometer performances, the INTERACT-II campaign has been performed at CIAO from July 2016 to January 2017 in the framework of the transnational access activities of the H2020 research infrastructure project ACTRIS-2 (Aerosol Clouds Trace gases Research InfraStructure, http://www.actris.eu). Aligned to those of INTERACT, the main

80 scientific objectives of INTERACT-II have been to:

➢ Evaluate the performance of commercial automatic lidars and ceilometers to measure the geometric and optical aerosol/cloud properties (with respect to the instrument sensitivity to different loads and types of aerosols and clouds);

➢ Assess the instrument Signal to Noise Ratio (SNR) and dynamic range (depending on the aerosol extinction

85 coefficient, water vapor content, solar irradiance, etc.);

➢ Study the instrument stability over time (e.g. laser, detector, efficiency, thermal drifts, etc.);

➢ Assess the ceilometers' calibration stability and accuracy (using an ACTRIS/EARLINET Raman lidar as a reference).

The campaign included an automatic lidar (MiniMPL, provided by Sigma Space Corporation), and four ceilometers

90 (Campbell CS135, VAISALA CT25K and CL51, and Jenoptik CHM15k).

INTERACT-II adopted the same philosophy and the methodological approach employed in the INTERACT campaign (Madonna et al., 2014) with the added value to intercompare at once the newest generation of 905-910 nm ceilometers, the MiniMPL lidar, recently delivered on the market, and the advanced multi-wavelength Raman lidars operated at CIAO, including the EARLINET reference mobile system, MUSA (Multi-wavelength System for Aerosol). The capability of lidars and ceilometers to detect aerosol layers and provide quantitative information about the atmospheric aerosol geometric and optical properties. Advanced Raman lidar measurements are provided by the two permanently deployed lidars operative at CIAO: MUSA, which is one of the mobile reference systems used in the frame of the EARLINET Quality Assurance Program, and PEARL (Potenza EArlinet Raman Lidar). Range corrected signals (RCS) of CIAO Raman lidars (hereinafter MUSA/PEARL) have been compared with those provided by the MiniMPL lidar, while the MUSA/PEARL attenuated backscatter coefficient profiles (β') have been compared with the corresponding β' profiles provided by ceilometers.

CHM15k and CT25K performances shown during INTERACT-II are not discussed in this paper because both the ceilometers have been already characterized during INTERACT (Madonna et al., 2014). In addition, from July to October 2016, the CHM15k underwent through a laser realignment, and the system has been mainly used during the last part of the campaign to perform a few stability tests of the laser which are described later on in the paper.

In the next section, we describe the instruments deployed during INTERACT-II. In section 3, the algorithms used for the data processing are presented. In Section 4, we show and discuss the intercomparison results between MUSA/PEARL and MiniMPL, while ceilometers' performances are described in Section 5. The stability of the ceilometers with respect to the changes in the environmental temperature is analyzed in Section 6. Summary and conclusions are finally provided.

2. Instruments

Located in the middle of the Mediterranean region, with proximity to the sea at less than 150 km in most directions and located in a strategic location with respect to the occurrence of African dust outbreaks and Eastern European forest fires, CIAO represents an ideal location for the observations of different aerosol species under different meteorological conditions. Beyond the multi-wavelength Raman lidars and the ceilometers mentioned in the introduction, CIAO utilizes a suite of instruments that provides continuous observation of the atmosphere including a microwave radiometer, a Ka-band cloud radar, a sun-star-lunar photometer. Moreover, radiosoundings are launched weekly (Madonna et al., 2011).

Ceilometers were installed on the roof of the observatory building (about 10m above the ground), while the MiniMPL, which is heavier and larger than a ceilometer, has been deployed close to MUSA and PEARL at the surface. Table 1 reports the specifications of the MiniMPL, MUSA and PEARL at 532 nm while Table 2 provides specifications for the infrared receivers of ceilometers, MUSA and PEARL.

MUSA is a mobile multi-wavelength lidar system based on a Nd:YAG laser source at 1064nm that it is doubled and tripled to add additional wavelengths at 532 and 355nm. The receiver unit is constituted by a Cassegrain telescope with a primary mirror of 300 mm diameter. The three laser beams are simultaneously and coaxially transmitted into the atmosphere beside the receiver in biaxial configuration. The receiving system has 3 channels to detect the elastically backscattered radiation from the atmosphere and 2 additional channels for Raman inelastically backscattered radiation by atmospheric N_2 molecules at 607 and 387 nm. The elastic channel at 532 nm is split into parallel and perpendicular polarization components by means of a polarizing beam splitter cube. The backscattered radiation at all the wavelengths is acquired by photomultiplier tubes both in analog and photon counting mode. The calibration of depolarization channels is automatically made using the ±45 method (Freudhentaler et al., 2009). The typical vertical resolution of the raw profiles is 3.75 m at 1 min temporal resolution. The MUSA system is compact and transportable and it is one of the reference systems employed for the EARLINET quality assurance program (Pappalardo et al., 2014).

The multi-wavelength lidar system for tropospheric aerosol characterization, PEARL (Potenza EArlinet Raman Lidar), has been designed to provide simultaneous multi-wavelength aerosol measurements for the retrieval of optical and microphysical properties of atmospheric particles as well as water vapour mixing ratio profiles. The system was operative according to regular EARLINET measurement schedule until 2014 and since then has been operated only for testing, during special events, and as back-up for the MUSA system when MUSA moves abroad for the calibration of the

Atmospheric
Measurement
Techniques
Discussions

EARLINET stations (Wandinger et al., 2016). PEARL is based on a 50 Hz Nd:YAG laser source emitting at 1064, doubled and tripled to 532 and 355 nm respectively. An optical system based on mirrors, dichroic mirrors and 2X beam
140   expanders separates the three wavelengths allowing optimization of the energy and divergence for each wavelength. The beams are mixed again for collinearity of the three wavelengths and to transmit them simultaneously and coaxially with respect to the lidar receiver. The backscattered radiation from the atmosphere is collected by an F/10 Cassegrain telescope (0.5m diameter, 5m focal length) and forwarded to the receiving system, equipped with 17 optical channels. Three channels are devoted to the detection of the radiation elastically backscattered from the atmosphere at the three laser
145   wavelengths, and three channels are used for the Raman radiation backscattered from the atmospheric N2 molecules at 387 nm and 607 nm and H_2O molecules at 407 nm. Two additional channels detect the polarized components of the 532 nm backscattered light. Each of these channels is further split into two channels differently attenuated for the simultaneous detection of the radiation backscattered from the low and high altitude ranges in order to extend and optimize the signal dynamic range. For the elastic backscattered radiation at 1064 nm the detection is performed by using an APD
150   detector and the acquisition is performed in analog mode. For all the other acquisition channels, the detection is performed by means of photomultipliers and the acquisition is in photon-counting mode. The vertical resolution of the raw profiles is 7.5 m for 1064 nm and 15 m for the other wavelengths, and the raw temporal resolution is 1 min.

The MiniMPL transceiver weighs 13 kg and measures 380 × 305 × 480 mm (width, depth, and height). The system consists of a laptop and the lidar transceiver, connected by a USB cable, and the average power consumption is about 100
155   W during normal operations. The whole system fits in a transportable storm case with a telescopic handle and wheels and can be checked in as regular luggage during a domestic or international flight. The MiniMPL's Nd:YAG laser emits polarized 532 nm light at a 2.5 KHz repetition rate and 3.5-4 µJ nominal pulse energy. The laser beam is expanded to the size of the telescope aperture (80 mm) to satisfy the eye safe requirements in ANSI Z136.1.2000 and IEC 60825 standards. The system also has built-in depolarization measurement (Flynn et al., 2007) with a contrast ratio greater than 100:1. The
160   receiver uses a pair of narrowband filters with bandwidth less than 200 pm to reject the majority of solar background noise. The filtered light is then collected by a 100 µm multimode fiber and fed into a Silicon Avalanche Photodetector operating in photon-counting mode (Geiger mode). Photon-counting detection enables the MiniMPL design to be lightweight and compact with high signal-to-noise ratio (SNR) throughout the troposphere. MiniMPL sets the laser beam divergence at about 40 µrad and receiver FOV at 240 µrad. This design balances the solar noise with optical system
165   stability and avoids multiple scattering which can distort measurements of depolarization ratio and extinction coefficient in the cloud.

The Vaisala Ceilometer CL51, in the second generation of Vaisala single lens ceilometers, is designed to measure high-range cirrus cloud base heights while maintaining the capability to measure low and middle range clouds and, in high turbidity conditions, vertical visibility. Its application to detection of tropospheric aerosol layers is under investigation in
170   several papers in literature (e.g. Wiegner et al., 2014). The CL51 employs a pulsed diode laser source emitting at 910±10 nm (at 25 ◦C with a drift of 0.27 nm K^{-1}) with a repetition rate of 6.5 kHz. The refractor telescope that employs an enhanced single lens technology theoretically allows reliable measurements virtually at surface, although the overlap correction estimated by the manufacturer is not able to effectively correct the ceilometer profile over the entire incomplete overlap region. The backscattered radiation is filtered using an optical bandpass filter which, according to Vaisala, is on
175   the order of 3.4 nm and then detected using an APD in analog mode. The instrument is used in INTERACT-II was updated with the latest firmware version (v1.034).

The Campbell scientific CS135 ceilometer employs a pulsed diode laser source emitting at 912±5nm with a repetition rate of 10 kHz. The ceilometer receiver is based on a single lens telescope. Half of the lens is used for the transmitter and the other for the receiver with a total optical isolation between them. The optical layout is conceived to enable lower
180   altitude measurement and to integrate larger optics into a compact package. Like the CL51, the backscattered radiation is filtered using an optical bandpass filter (36 nm) and detected using an APD in analog mode. The latest version of the instrument firmware was provided by the manufacturer itself. During INTERACT-II, CS135 data collection (performed using a terminal emulator) was affected by a technical problem with the CIAO logging system which caused the loss of a large amount of data especially in the free troposphere, thus limiting the number of available cases for the comparison
185   (only 9 measurement sessions).

At this stage, it is worth providing a few clarifications about the hybrid nature of this intercomparison campaign which involved both automatic elastic (polarized) lidars and regular ceilometers. As remarked upon in Madonna et al. (2015),

Atmospheric
Measurement
Techniques
Discussions

ceilometers are optical instruments based on the lidar principle but eye-safe and generally lower in cost and performance compared to advanced research or automatic elastic lidars. Their primary application is the determination of cloud base height and vertical visibility for transport-related meteorology applications. These instruments typically have SNRs considerably lower than lidars because they employ diode lasers and wider optical bandpass filters to detect over the broader spectrum of these sources. The use of these sources is often permitted only if they observe eye-safety limits which allow to operate ceilometers unattended. In a few more powerful ceilometers, like the CHM15k and CHM15kx, as well as the MPLs (including MiniMPL), the use of diode-pumped lasers allows much larger SNRs and therefore enhanced performances (e.g. Madonna et al., 2014). Moreover, ceilometers, while providing factory calibrated attenuated backscatter profiles, do not often provide the raw backscattered signals and their processing software includes several automatic adjustments of the instrument parameters (e.g. gain, voltages, background suppression, etc.) performed according the observed scenario (e.g. daytime, night time, clear sky or cloudy) but out of the control of users. This makes it difficult to use them for research purposes beyond the applications for which they were designed.

During INTERACT-II, a hybrid ensemble of these instruments, automatic lidars and ceilometers have been deployed. Nevertheless, the main scope of the campaign remains the assessment of the performances of each different category of instruments separately, and, within the same category, to assess the limitation in the use of each system involved. Therefore, the results presented in section 4 and 5 are intended to show under which limitations each of the investigated systems is able to provide quantitative information on the aerosol properties in both the boundary layer and in the free troposphere. The reader should use these results according to his or her own specific needs and with careful consideration of the application.

3. Intercomparison methodology and data processing.

Following the same approach used during INTERACT, MUSA/PEARL signals have been processed using the EARLINET Single Calculus Chain (SCC) (D'Amico et al., 2016; Mattis et al., 2016). The SCC outputs are the pre-processed range corrected signals (RCS) and the profiles of aerosol extinction coefficient at 355 and 532 nm and backscattering coefficient at 355, 532 and 1064 nm, using both Raman and elastic signals.

Differently from ceilometers, the MiniMPL also provides the raw signals, acquired in photon counting mode only, enabling the direct comparison with the MUSA/PEARL signals. RCS is a quantity proportional to the attenuated backscattering β', which is used for the investigation of ceilometer performance, and allows a comparison between the two systems over a vertical range larger than the range where β' is available. This is because the β' calculation depends on the range covered by the retrieval of the MUSA/PEARL extinction coefficient using the Raman method, applied in this work, which cover a shorter vertical range because of the lower SNR typical of the Raman lidar channels. The use of RCS brings the comparison to the signal level, avoiding calculation of higher level products whose retrieval can increase the number of assumption and uncertainties (e.g. Lolli et al., 2017).

To perform the comparison, the 532 nm MiniMPL RCS is normalized to the corresponding MUSA/PEARL RCS over a vertical range of 1.2 km starting from a variable reference altitude between 6 and 8 km asl, where the aerosol content is identified as negligible using quicklooks of the lidar time series. All the time series considered in this comparison refer to night time clear sky measurements. The profiles from all the instruments are compared over a vertical resolution of 60 meters and a temporal integration time ranging from 1 to 2 hours, selected automatically by the SCC depending on the observed atmospheric scenario. No vertical smoothing is applied to the data processing, but systems outputting data at a higher resolution are interpolated at the MUSA/PEARL resolution. All of the profiles are cut in the lower part of the atmosphere, below 1300 m asl, in order to consider MUSA/PEARL reference lidar signals only in the region with the full overlap between the telescope and laser beam. The number of the simultaneous MUSA/PEARL and MiniMLPL measurements time series has been limited by a few periods of unavailability of the MiniMPL due to an issue in the regulation of the instrument housing thermostat.

For the ceilometers, the comparison was carried out using the 1064 nm β' profiles obtained through their normalization over the corresponding MUSA/PEARL β' profile below 3 km asl over a vertical range of 600 m, where the full overlap of all instruments was ensured. Given that ceilometer measurements are performed at 910-912 nm, β' profiles have been rescaled using the 532/1064 beta-related Angstrom coefficient measured by MUSA/PEARL in order to obtain the

Atmospheric
Measurement
Techniques
Discussions

Open Access

EGU

equivalent profile at 1064 nm for comparison with MUSA/PEARL. For those altitudes where the beta-related Angstrom coefficient was not available (more frequently in the free troposphere (FT), above 5 km asl) a climatological value of 1.05 was used. The uncertainty due to the use of the 532/1064 beta-related Angstrom coefficient instead of the 905/1064 coefficient is assumed to be lower than 1 % (Wiegner et al., 2015). More details on calibration are discussed in section 5.

240 A ceilometer β' profile can only be retrieved if water vapor absorption is taken into account (Wiegner et al., 2015). The influence of water vapour absorption at operating wavelengths of ceilometers is due to the presence of a strong absorption band between 900 and 930 nm, while at 1064 nm there is no absorption. Therefore, the retrieval of β' profiles must consider the water vapour attenuation. In this study, water vapor correction has been estimated using Fu-Liou-Gu (FLG) radiative transfer model (Gu et al., 2011), in the modified version discussed in Lolli et al. (2017b).

245 FLG is a combination of the delta four-stream approximation for solar flux calculations (Liou, 1986) and a delta-two-four-stream approximation for IR flux calculations. The solar (0–4 μm) and IR (4–50 μm) spectra are divided into 6 and 12 bands, respectively, according to the location of prominent atmospheric absorption bands. FLG makes use of the adding procedure to compute the spectral albedo in which the line-by-line equivalent radiative transfer model (Liou et al. 1998) uses the correlated k-distribution method for the sorting of absorption lines in the solar spectrum. In the solar
250 spectrum, non-gray absorption due to water vapor, O_3, CO_2, O_2, and other minor gases, such as CO, CH_4, and N_2O, is taken into account. Non-gray absorption due to water vapor, O_3, CO_2, CH_4, N_2O and CFCs is considered in the IR spectrum. Potenza GRUAN processed (collocated) radiosoundings were used as input for the FLG radiative transfer model (Lolli et al., 2017a) in about 40% of the cases while for the remaining cases when local radiosondes were not available, data from closest RAOB site located in Brindisi Casale (40.63N, 17.94E, 15 m) about 150 km east of Potenza
255 were used. RAOB profiles were cut at the CIAO altitude level (760 m). According to the correction method suggested in literature for 905-910 nm ceilometers (Wiegner et al., 2015), an optimal correction would require the knowledge of both the laser wavelength and the bandwidth for each emitted pulse. These data are not currently stored and provided by the ceilometer hardware. Therefore, to estimate the water vapor correction a laser Gaussian profile centered at the nominal laser wavelength with a FWHM of 3.5 nm has been assumed. Moreover, FLG has a spectral resolution of 50 cm^{-1} while
260 in literature a resolution lower than 0.2 cm^{-1} is recommended to avoid an "unpredictable" behavior of the model calculation. The water vapor absorption has been calculated as the average absorption within the spectral range described above. In addition, the comparison between the ceilometers and the lidars, discussed in section 5, shows that the uncertainty due to the water vapor correction cannot represent the main contribution to the total uncertainty budget of 905-910 nm ceilometer measurements.

265 For the comparison between MUSA/PEARL and MiniMPL, it is important to remark that MUSA detects with two channels the co- and cross polarized components of the elastically backscattered radiation at 532 nm, in order to measure the particle depolarization at that wavelength. MiniMPL also detects the co- and cross polarized components of the elastically backscattered radiation at 532 nm and provides continuous measurements of particle backscattering coefficient and depolarization ratio profiles. Because of different polarization setups, MUSA measures the particle linear
270 depolarization ratio (Freudenthaler et al., 2009) while mini-MPL measures the particle circular depolarization (Flynn et al., 2007). For both MUSA and MiniMPL, total signals must be calculated for through the combination of the respective co- and cross-polarized channels. 532nm MiniMPL RCS has been calculated according to the equations provided in Campbell et al. (2002). PEARL, instead, is equipped not only with the co- and cross-polarized channels at 532 nm but also with channels detecting the 532 nm total backscattered radiation.

275 To provide a first examples related to the datasets discussed in this paper, a comparison of the 532 nm PEARL RCS and MiniMPL normalized relative backscatter (NRB) at their own time and vertical raw resolutions is shown in Figure 1 for the measurements collected on 13 October 2016 from 18:00 to 19:00 UT; NRB is equivalent to pre-processed PEARL RCS except for a constant factor. Figure 2 shows the comparison of the 1064 nm PEARL RCS with the 910-912 nm CL51/CS135 attenuated backscatter for the same day. To ensure correct interpretation of Figures 1 and 2, it is important
280 to reiterate that PEARL raw time and vertical resolutions are of 1 minute and 15 m, for MiniMPL resolution are of 5 minutes and 30 m, for CL51 are of 10 m and 30 seconds, and for CS135 are of 5 m and 30 seconds.

Finally, it is also important to note that the CIAO operator during INTERACT-II practiced routine checks to allow each of the involved instruments to perform as close as possible to the manufacture specifications. The routine maintenance included:

Atmospheric
Measurement
Techniques
Discussions

285   a.   A daily inspection of instrument and its operation;

  b.   A weekly check-up of instrument acquisition parameters (laser transmitter, receiver, heater, blower, windows, tilt angle, etc.);

  c.   Approximately bi-weekly cleaning of the window, with frequency depending on atmospheric conditions (e.g.
290   after precipitation or dust/smoke transport events) using a water flash flooding and specific treatments to remove the stronger dust spots, additionally performed in response to warning messages provided by each instrument (e.g. window contamination messages);

  d.   Dark current measurements twice during the campaign for ceilometers, using a termination hood provided by the manufacturer while operating in analog detection mode. Dark current profiles were subtracted from each of
295   the raw backscatter profile before normalization over the lidar; for MUSA and PEARL, dark currents are routinely estimated before each measurements session.

4. MiniMPL vs MUSA: Comparison of Range-corrected signals

Simultaneous observations of the multi-wavelength Raman lidars operative at CIAO, MUSA and PEARL, and of the
300 automatic Sigma Space mini-MPL, collected during the measurement campaign, have been compared.

An example of comparison between RCS provided by MUSA and mini-MPL is shown in the left panel of Figure 3, related to the observations collected on 29 August 2016 from 19:16 to 20:47 UT. The quicklooks of the RCS time series (not reported) show a sharp aerosol layer between about 1.5 km and 2.5 km asl along with a lower aerosol loading below the layer to the ground, while the atmosphere is dominated by the molecular scattering above. In the right panel of Figure 3,
305 the air mass back trajectory analysis performed using the NOAA HYSPLIT model started at the three levels from the ground to the highest layer observed by both MUSA and MiniMPL lidars. Trajectories are obtained using the vertical velocity model of HYSPLIT running the backtrajectories for a length of 200 hours at three vertical levels (ground level, 1000 m and 2000 m asl).

The difference between the two profiles shows a very good agreement throughout the troposphere with discrepancies <
310 5% between 2.0 km and 4.0 km asl, within the RCS random uncertainty. MiniMPL underestimates MUSA (up to 10% RCS) at altitudes lower than 2.0 km asl, in the incomplete overlap region. MiniMPL data processing provides a correction function which is not able to properly adjust all of the collected signals in the incomplete overlap region. The beam pointing instability of the laser in this vertical range is likely the reason preventing the adjustment using a precomputed static correction function.

315 A second example is provided in the left panel of Figure 4, which shows observations collected on 29 August 2016 from 19:56 to 21:45 UT. Multiple aerosol layers up to 4.0 km asl are observed. In the right panel of Figure 4, the corresponding air mass back trajectory analysis shows the quasi-zonal transport of the observed aerosol over from North-East Canada over the Atlantic Ocean to Europe. Also in this case, the comparison shows a very good agreement throughout the troposphere with discrepancies <5%. Differences in the incomplete overlap region are again observed but a small
320 difference can be noted also above this region and up to 4.0 km of altitude, where most of the aerosol loading is located. This difference might be related to the uncertainty affecting the estimation of other corrections applied to the MiniMPL data processing, e.g. after-pulse correction. Nevertheless, the differences are within the RCS random uncertainty and do not compromise the good agreement between the two systems.

In Figure 5, the black line shows the profile of the average fractional difference between MUSA and MiniMPL values of
325 RCS calculated for 12 cases of simultaneous and collocated measurements collected in the period from July to December 2016. The vertical bars are the standard deviations of average fractional differences. The profile shows that MiniMPL underestimates MUSA in the region below 2.5-3.0 km with an increasing average difference towards ground level; the maximum value of this deviation is less than 15%. The blue line reported in Figure 5 represents the same as the black line but adjusted by applying an additional overlap correction factor to the MiniMPL, estimated using the ratio between MUSA
330 and MiniMPL profiles during the cleanest simultaneous measurement session available during INTERACT-II. The additional correction applied from the ground to 3.3 km asl, identified as the overlap height for the MiniMPL, reduces

Atmospheric
Measurement
Techniques
Discussions

the average differences to less than 3% from 1.8 km to 3.3 km and the standard deviation of the difference keeps to within 10%. Below 1.8 km, the correction is not able to properly adjust the profile due to the presence of the aerosol residual layer in the measurements used to estimate the correction factor. The example correction for the overlap effects provided in Figure 5 cannot be considered exhaustive but demonstrates that some work is required to improve the MiniMPL data processing in the incomplete overlap region. In the remainder of this section, the MiniMPL original data processing will be considered.

The good stability of the MiniMPL calibration ("lidar normalization") during the campaign is shown by the small variability (10%) of differences in the normalization region, typically between 6 km and 8 km asl. This also confirms the good stability of MiniMPL in its operation in the considered time period and with respect to seasonal changes in the environmental temperature and in the aerosol loading.

In Figure 6, the comparison of the MUSA and MiniMPL probability density functions (pdfs) of the RCS values confirms the overall good agreement between MUSA and mini-MPL, with some tendency of mini-MPL to overestimate MUSA for RCS values lower than 1.5 1010 (a.u.): this difference is more evident in the left panel of Figure 6, where pdfs are calculated for the vertical range below 4 km asl.

Finally, in Figure 7, the relationships between the 532 nm aerosol extinction coefficient (α_{par}) from MUSA and PEARL lidars and the corresponding RCS at 532 nm measured by MUSA and PEARL lidars and by MiniMPL is shown to highlight differences in lidar sensitivity to different aerosol types, i.e. different aerosol extinction coefficients. α_{par} is calculated over the same temporal window as RCS, but with a lower effective vertical resolution (typically within 480-600 m) in order to reduce the uncertainty and the related oscillation affecting the extinction profile calculated using the Raman lidar signal. The output profile vertical resolution is 60 m to match the RCS vertical resolution. The comparison in Figure 7 shows a good agreement between MiniMPL and MUSA. The most evident differences between the two lidars can be identified for values of α_{par} larger than about $5.0 \ 10^{-5} \ m^{-1}$ where MiniMPL shows a broader scatter of the RCS values, not observed for CIAO lidars. In particular, for the RCS values smaller than $1.0 \ 10^{10}$ (low signals), this is likely due to inaccurate adjustments applied to the signals processing, described above, which generates a sort of systematic effect in the free troposphere. For values of RCS larger than $1.0 \ 10^{10}$, the difference between the two lidars is due to the profile discrepancies in the incomplete overlap region between 1.0 km and 3.3 km asl.

5. Ceilometer: Comparison of attenuated backscattering

This section focuses on the comparison of attenuated backscattering (β') simultaneously measured by MUSA and PEARL multi-wavelength Raman lidars and estimated for the CL51 and the CS135 ceilometers. The left panel of Figure 8 shows the attenuated backscatter retrieved from MUSA, CL51 and CS135 on 13 October 2016 in the time interval from 17:47 to 19:08 UT. The HYSPLIT air mass back trajectory analysis (not shown) reveals that the observed advected aerosol layers may come from Libya and Morocco, two regions where large sources of dust are present for the different altitude levels. The agreement between the three instruments is extremely good below 2.5 km asl. Between 2.5 and 3.7 km asl there are differences for both the CL51 and the CS135 with larger difference shown by the CS135. The difference between the CL51 and CS135 2.5 and 3.5 km asl may be also partly affected by the dependency of the water vapour correction on the emitted laser spectrum. The CS135 SNR strongly decreases above 3.5 km close to the top region of the second observed aerosol layer. The CL51 SNR is higher but not sufficient to reliably detect the residual aerosol backscattered radiation at that altitude ranges as well the molecular return. All the CL51 profiles shown in Figure 8 below are cut below 5.0 km asl, to better visualize the comparison otherwise affected by the large noise oscillation of the signals.

The right panel of Figure 8 shows attenuated backscatter measured by the same instruments on 01 December 2016 from 17:53 to 19:19 UT. The backtrajectory analysis for this time period showed that the observed air mass originated in Canada and reached CIAO via North-West Europe. This comparison reveals the effect of ceilometer variability in the region of incomplete overlap: the correction applied by the manufacturer is often able to adjust the profile minimizing the difference with MUSA, but in many other cases those differences with MUSA are considerable. It is worth reiterating that, as for the MiniMPL comparison, all the profiles are cut off below 1.3 km asl because MUSA is considered the reference signal only in the full overlap region.

Atmospheric
Measurement
Techniques
Discussions

380   Regarding the CL51 β' profiles, the choice of normalization range has proven to be more critical than expected. Initially, all the CL51 profiles were normalized over a 0.6 km vertical range below 8 km asl in order to find a trade-off between an acceptable CL51 SNR and the need to normalize in a stable aerosol free region. Nevertheless, the CL51 SNR is too low in the FT and the decrease in its sensitivity to the molecular return makes the normalization to the lidar in the FT (and consequently the ceilometer molecular calibration) challenging. The left panel of Figure 9, shows the comparison between
385   β' retrieved from MUSA and CL51 on 4 July 2016 from 19:56 to 21:45 UT using two different normalization ranges, the first below 3 km and the second below 4.3 km, over a 0.6 km normalization range. Both the raw calibrated profiles and the water vapor corrected calibrated profiles are shown. In the right panel of Figure 9, the MUSA 1064 nm RCS measured during the same time is shown. The aerosol layer observed up to 3.5 km asl arrived with air masses moving through a zonal transport above the Atlantic Ocean and then over Northern-Central Africa, and likely includes transported mineral
390   dust. Figure 9's left panel comparison clearly reveals that, due to the very low SNR for the CL51 above 3.5 km asl, the molecular calibration is challenging and may result in systematic errors on the retrieved profiles. Aside from the stratocumulus cloud calibration, not addressed in this work, the only possible CL51 normalization to provide a reliable estimation of β' must be performed over a profile of β' retrieved from a reference lidar (like MUSA or PEARL).

       CL51 and CS135 dark currents were subtracted from each ceilometer vertical profile to subtract instrumental artefacts
395   affecting the signals, especially in the free troposphere, and to test the feasibility of calibrating ceilometers using the molecular profile. In the CS135, the lack of information in the free troposphere due to data logging problems affected the measured dataset. For the CL51, dark current subtraction significantly reduces the distortions affecting the profiles in the free troposphere. Nevertheless, the ceilometer β' profile calculated for the 5 December 2016 from 17:53 to 19:19 UT (Figure 10), after the dark current subtraction, still has large differences in shape with respect to the PEARL profile, which
400   was successfully calibrated using a molecular profile. The comparison reveals that after dark current subtraction the CL51 β' becomes negative below 4.5 km asl indicating that the measured dark currents are inadequate to correct for the signal distortion along the entire profile. This kind of scenario is common throughout the INTERACT-II dataset. The choice of the measurement collected on 5 December 2016 in not random, but it is the closest available case to the measurements of dark currents, which was performed on 22 December 2016 from 16:00 to 16:20 UTC for the CL51.

405   It is worth clarifying that a more frequent measurement of dark current over a longer time window could improve the correction of the signal distortion affecting the ceilometer β' profiles in the free troposphere. Measuring the dark current every 12 hours (once for nighttime and once for daytime measurements), and over a longer integration time, i.e > 1-2 hours, might enable successful application of the molecular calibration. The best practice for performing these measurements, though primarily of interest to the lidar research community, could be assessed for ceilometers in
410   cooperation with the manufacturers in order to improve dark current correction and allow a more accurate molecular calibration. Tests to assess the value of performing appropriate dark measurements to enable the molecular calibration for the 905-912 nm ceilometers is currently under investigation through analysis of the database collected during the CeiLinEX Campaign (Mattis et al., 2017).

       The left panel of Figure 11 shows the profile of the average fractional difference between MUSA/PEARL and CL51
415   values of RCS calculated for 19 cases of simultaneous and collocated measurements, while on the right panel the same is shown for the CS135 but calculated only for 9 cases. The vertical bars again represent the standard deviations of average fractional differences. The profiles have been cut off at about 3.5 km asl for both ceilometers because of the low number of available cases with a sufficient high SNR above that altitude. The CL51 underestimates MUSA/PEARL in the region below 2.0 km asl with a difference lower than 20-30 %. It overestimates MUSA/PEARL above 3.0 km, where the
420   decrease of the CL51 SNR with altitude does not allow the normalization in the FT and the differences with MUSA/PEARL increases to 40-50 %. In the region between 2.0 and 3.0 km asl, where the normalization is applied, the difference is within 10 %; in this region, the variability vertical bar is also indicative of the stability of the normalization costant, which is within 30 %. For the CS135, the performances are similar to the CL51 in the region below 2.0 km asl, while in the region above 3 km asl the difference with MUSA/PEARL is variable and within ±40 %. The standard
425   deviation of the normalization constant is within 40-50 %.
       Figure 12 shows the pdfs of the β' values measured or estimated by MUSA/PEARL and CL51, in the left panel, and by MUSA/PEARL and CS135, in the right panel. The pdfs are limited to β' values below 4 km asl due to the SNR decrease of both the instruments (see above). The intercomparison confirms the agreement between MUSA/PEARL and both ceilometers for the higher values of β', while for lower values, below 0.2-0.3 10^{-6} $m^{-1}sr^{-1}$, the differences are more
430   pronounced due to the ceilometers' lower SNRs.

Atmospheric
Measurement
Techniques
Discussions

Finally, Figure 13 shows the scatterplots of the relationship between 532 nm aerosol extinction coefficient and 1064 nm attenuated backscattering for CL51 vs MUSA/PEARL in the left and right top panels, respectively, while for CS135 and MUSA/PEARL in the left and right bottom panels, respectively. The scatterplots include just the values measured below 3.5 km asl. For the CL51, differences with MUSA in the scatter plot are small and mainly related to the region where β'

435 $< 5.0 \ 10^{-7} \ \text{m}^{-1} \ \text{sr}^{-1}$ and $\alpha_{par} > 8.0 \ 10^{-5} \ \text{m}^{-1}$: in this region, the values observed by MUSA correspond to very small values detected by the CL51. For the CS135, though a small number of cases are available an effect similar to the CL51 can be identified in the region where β' $< 5.0 \ 10^{-7} \ \text{m}^{-1} \ \text{sr}^{-1}$ and $\alpha_{par} > 5.0 \ 10^{-5} \ \text{m}^{-1}$; these threshold values reveal the slightly better performance of the CL51 when the values of α_{par} are larger for corresponding small values of β' and, therefore, indicates its improved SNR in the FT which corresponds to the reported values.

440

6. Ceilometer stability

In the previous sections, the overall stability of ceilometers' calibration constant calculated in this paper has been addressed in a statistical sense. The use of two different multi-wavelength Raman lidars during INTERACT-II did not

445 permit evaluation of the stability of the ceilometer calibration constant in comparison with the lidar system molecular calibration constant, nor did it permit in depth assessment of calibration stability in relation to other parameters (e.g. ambient temperature, aerosol optical depth, etc). Though the MUSA and PEARL lidars were compared in the past and may be used almost indifferently to measure aerosol optical properties, their experimental setups are quite different and therefore different calibration constants are required for the two systems.

450 Nevertheless, following from the results of INTERACT-I and in order to assess stability of ceilometer calibration over the time, a few tests and studies were performed using the CHM15k as a test-bed. The system (already successfully tested during INTERACT-I) was not available for much of INTERACT-II due to major maintenance from July to October 2016, so was devoted to this auxiliary testing role taking advantage to the ancillary information provided by the manufacturer through the CHM15k acquisition software. A few tests revealed a not negligible sensitivity of the laser to changes in the

455 ceilometer's enclosure temperature. These changes affect the number of laser pulses emitted per measurement cycle and they are correlated with changes in ambient temperature. To investigate the effect of this behavior on the ceilometer data processing, the whole CHM15k historical dataset available at CIAO was studied. In particular, in Figure 14 the number of laser pulses per measurement cycle (30 s) is shown as a function of time from 2010 to 2016. The CHM15k laser specification provided by the manufacturer is consistent with the measured laser pulse variability, less than <10%.

460 Occasionally, values up to 15-20 % are also detected. The specified nominal pulse-to-pulse variance of laser energy is lower than 3%. Interestingly, the laser pulse count variability of 10% does not occur in a random way but, instead, follows a clear dependence on the environmental temperature. Presumably the ambient temperature affect the ceilometer enclosure temperature, which has the effect of increasing the number of laser pulses in summer and a decreasing the number in winter. The number of lasers pulses is assimilated as a multiplying factor in the CHM15k data processing and

465 in general is embedded in the so-called lidar constant within the lidar equation. As a consequence, the temperature dependence shown by the laser pulses, likely not unfamiliar to laser experts, directly affects the received signal with a SNR decrease in cooler temperatures and, therefore, increases the uncertainty of any type of calibration method applied to retrieve the aerosol optical properties from the ceilometer's data.

This indicates that, across a fixed calibration range (i.e an aerosol free range to perform the molecular calibration), the

470 calculated embedded constant will show the same seasonal variability shown by the laser pulses in order to correct for the change in transmitted energy. This partly explains what was reported during INTERACT (Madonna et al., 2015), but only partly justifies the large variability of the calibration constant (about 58 %) calculated during the six-month period of INTERACT-I. The reported seasonal behavior also confirms that the evaluation of the ceilometer calibration over a period longer than 6 months will provide an additional uncertainty in the calibration constant of 10-20 %; over a period

475 of three months the additional uncertainty may reduce to 5-10%. A similar behavior has been observed for the other ceilometers during INTERACT and INTERACT-II but both the unavailability of single reference lidar during INTERACT-II as well as the limited database available (only 6 months) did not allow this analysis to be extended to the other ceilometers. It is worth remarking that this seasonal variability has a limited effect on the retrieval of β' for those calibration methods which allows a frequent or continuous calibration (e.g. molecular calibration or indirect calibration

480 using ancillary measurements from a sun photometer); for these methods, the intrinsic accuracy of the calibration method itself is more relevant and can provide the largest uncertainty contribution.

7. Conclusion and outlook

485 During the INTERACT-II, the newest generation of 905-910 nm ceilometers, the MiniMPL lidar were compared with the CIAO EARLINET multi-wavelength Raman lidars, MUSA and PEARL.

The MiniMPL agrees with the CIAO lidars to within 10-15 % and most of the differences could be reduced after a re-evaluation of the overlap correction applied in the data processing. A preliminary evaluation of the new correction function has been done during the campaign by using the ratio between MiniMPL and MUSA in the cleanest night time simultaneous measurements available from both lidars. Nevertheless, a more accurate evaluation of the MiniMPL overlap
490 correction function must be carried out by the manufacturer.

The CL51 ceilometer showed a much better performance than the previous generation of VAISALA ceilometers. The CL51 is able to detect the molecular signal in the free troposphere, thus enabling the calibration of attenuated backscatter on a molecular profile to retrieve the aerosol backscattering coefficient over an integration time of 1-2 hours. Nevertheless, signal distortions can have a large effect on the molecular calibration even after dark current subtraction. For this reason,
495 normalization to the multi-wavelength Raman lidar measurements has been performed below 3.0 km asl. Stability of the CL51 calibration constant was within 30 %.

The CS135 showed improvements compared to the prototype tested during INTERACT-I. Its performance was similar to the CL51 in the region below 2.0 km asl (within 20-30% of the MUSA/PEARL attenuated backscatter). However, in the region above 3.0 km asl the differences are ±40 % and molecular calibration is still not feasible for this ceilometer.
500 Stability of CS135 calibration constant is within 40-50 %.

Note that both ceilometers have been corrected for the effect of the water vapor absorption bands at their operating wavelengths. In addition, it is worth to point out that the reduced aerosol detection for CL51 and CS135 is also partly due instrumental processing mainly optimized for cloud detection.

Finally, following the primary investigation conducted during INTERACT-II, a study of the CHM15k historical dataset
505 available at CIAO from 2010 to 2016 has revealed a variability of about 10% for the number of emitted laser pulses which, though within the manufacturer's specification, clearly depends on temperature, with an increase in the number of laser pulses in summer and a decrease in winter. The seasonal behavior shown by the laser pulse numbers directly affects the measured signal with increasing the uncertainty of any type of calibration method. This partly explains what was reported during INTERACT (Madonna et al., 2015), but only partly justifies the large variability of the CHM15k
510 calibration constant (about 58 %) calculated during the six-month period of INTERACT-I. The reported seasonal behavior also confirms that ceilometer calibration must be evaluated at minimum every 3-6 months to reduce the uncertainties.

The dataset during INTERACT-II will be made available the users upon request to the authors though the intention is to make to data available also through the ACTRIS data portal.

8. Acknowledgements

9. References

Campbell, J. R., D. L. Hlavka, E. J. Welton, C. J. Flynn, D. D. Turner, J. D. Spinhirne, V. S. Scott, and I. H. Hwang, Full-time, eye-safe cloud and aerosol lidar observation at Atmospheric Radiation Measurement Pro- gram sites: Instruments and data processing, J. Atmos. Oceanic Technol., 19, 431–442, 2002.

D'Amico, G., Amodeo, A., Mattis, I., Freudenthaler, V., Pappalardo, G.: EARLINET Single Calculus Chain technical: Part 1: Pre-processing of raw lidar data, Atmos. Meas. Tech., 7, 1979–1997, 2016.

Atmospheric
Measurement
Techniques
Discussions

Freudenthaler, V., Esselborn, M., Wiegner, M., et al.: Depolarization ratio profiling at several wavelengths in pure Saharan dust during SAMUM 2006, Tellus B, 61, 165–179, 2009

Flynn, C.J., Mendoza, A., Zheng, Y., Mathur, S.: Novel polarization-sensitive micropulse lidar measurement technique, Optics Express, 15, 2785-2790, 2007.

530   Gu Y, Liou KN, Ou SC, Fovell R,: Cirrus cloud simulations using WRF with improved radiation parametrization and increased vertical resolution, J. Geophys. Res.116:D06119, 2011.

Kotthaus, S., O'Connor, E., Münkel, C., Charlton-Perez, C., Haeffelin, M., Gabey, A. M., and Grimmond, C. S. B.: Recommendations for processing atmospheric attenuated backscatter profiles from Vaisala CL31 ceilometers, Atmos. Meas. Tech., 9, 3769-3791, https://doi.org/10.5194/amt-9-3769-2016, 2016.

535   Lolli S., Campbell, J. R., Lewis, J. R., Gu, Y., and Welton, E. J.: Technical note: Fu–Liou–Gu and Corti–Peter model performance evaluation for radiative retrievals from cirrus clouds, Atmos. Chem. Phys., 17, 7025-7034, https://doi.org/10.5194/acp-17-7025-2017, 2017a

Lolli, S., Madonna, F., Rosoldi, M., Campbell, J. R., Welton, E. J., Lewis, J. R., Gu, Y., and Pappalardo, G.: Fu-Liou Gu radiative transfer model used as proxy to evaluate the impact of data processing and different lidar measurement techniques in view of next and current lidar space missions, Atmos. Meas. Tech. Discuss., https://doi.org/10.5194/amt-540   2017-182, in review, 2017b.

Madonna, F., Amodeo, A., Boselli, A., Cornacchia, C., Cuomo, V., D'Amico, G., Giunta, A., Mona, L., and Pappalardo, G.: CIAO: the CNR-IMAA advanced observatory for atmospheric research, Atmos. Meas. Tech., 4, 1191–1208, 2011.

Madonna, F., Amato, F., Vande Hey, J., and Pappalardo, G.: Ceilometer aerosol profiling versus Raman lidar in the frame 545   of the INTERACT campaign of ACTRIS, Atmos. Meas. Tech., 8, 2207-2223, https://doi.org/10.5194/amt-8-2207-2015, 2015.

Mattis, I., D'Amico, G., Baars, H., Amodeo, A., Madonna, F., Iarlori, M.: EARLINET Single Calculus Chain technical Part 2: Calculation of optical products, Atmos. Meas. Tech., 9, 3009–3029, 2016.

Mattis, I., et al.: The international ceilometer inter-comparison campaign CeiLinEx2015 - uncertainties and artefacts of 550   aerosol profiles, European Meteorology Society (EMS) annual meeting, EMS2017-527, 2017

O'Connor, E. J., Illingworth, A. J., and Hogan, R. J.: A technique for autocalibration of cloud lidar, J. Atmos. Ocean. Tech., 21, 777–786, 2004.

Pappalardo, G., Amodeo, A., Apituley, A., Comeron, A., Freudenthaler, V., Linné, H., Ansmann, A., Bösenberg, J., 555   D'Amico, G., Mattis, I., Mona, L., Wandinger, U., Amiridis, V., Alados- Arboledas, L., Nicolae, D., and Wiegner, M.: EARLINET: towards an advanced sustainable European aerosol lidar network, Atmos. Meas. Tech., 7, 2389–2409, doi:10.5194/amt-7-2389- 2014, 2014.

Sawamura, P., J-P. Vernier, J.-E. Barnes, T. A. Berkoff, E. J. Welton, et al.: Stratospheric AOD after the 2011 eruption of Nabro volcano measured by lidars over the Northern Hemisphere. Environmental Research Letters, IOP Publishing, 560   2012, 7 (3), pp.034013.

Vande Hey, J., Coupland, J., Foo, M., Richards, J., and Sandford, A.: Determination of overlap in lidar systems, Appl. Optics, 50, 5791–5797, 2011.

Wandinger, U., Freudenthaler, V., Baars, H., Amodeo, A., Engelmann, R., Mattis, I., Groß, S., Pappalardo, G., Giunta, A., D'Amico, G., Chaikovsky, A., Osipenko, F., Slesar, A., Nicolae, D., Belegante, L., Talianu, C., Serikov, I., Linné, H., 565   Jansen, F., Apituley, A., Wilson, K. M., de Graaf, M., Trickl, T., Giehl, H., Adam, M., Comerón, A., Muñoz-Porcar, C., Rocadenbosch, F., Sicard, M., Tomás, S., Lange, D., Kumar, D., Pujadas, M., Molero, F., Fernández, A. J., Alados-Arboledas, L., Bravo-Aranda, J. A., Navas-Guzmán, F., Guerrero-Rascado, J. L., Granados-Muñoz, M. J., Preißler, J., Wagner, F., Gausa, M., Grigorov, I., Stoyanov, D., Iarlori, M., Rizi, V., Spinelli, N., Boselli, A., Wang, X., Lo Feudo, T.,

Atmospheric
Measurement
Techniques
Discussions

570   Perrone, M. R., De Tomasi, F., and Burlizzi, P.: EARLINET instrument intercomparison campaigns: overview on strategy
        and results, Atmos. Meas. Tech., 9, 1001-1023, https://doi.org/10.5194/amt-9-1001-2016, 2016.

        Wiegner, M., Madonna, F., Binietoglou, I., Forkel, R., Gasteiger, J., Geiß, A., Pappalardo, G., Schäfer, K., and Thomas,
        W.: What is the benefit of ceilometers for aerosol remote sensing? An answer from EARLINET, Atmos. Meas. Tech., 7,
        1979–1997, doi:10.5194/amt-7-1979-2014, 2014.

        Wiegner, M. and Gasteiger, J.: Correction of water vapor absorption for aerosol remote sensing with ceilometers, Atmos.
575   Meas. Tech., 8, 3971-3984, https://doi.org/10.5194/amt-8-3971-2015, 2015.

580

585

590

595

Atmospheric
Measurement
Techniques
Open Access
Discussions
EGU

600 **Table 1**: Specifications of MUSA, PEARL and MiniMPL lidars at 532 nm. All the lidars are operated in the zenith pointing mode. RFOV indicates the half-angle rectangular field of view of the instruments.

Instrument	Wavelength (nm)	Pulse Energy (µJ)	Repetition Rate (kHz)	Configuration	Laser Divergence (mrad)	RFOV (mrad)	Approx. Full Overlap Height (m)
MUSA	532	2.5×10^5	0.02	Biaxial	0.3	0.5	400
PEARL	532	5×10^5	0.05	Monoaxial	0.125	0.5	550
MiniMPL	532	3.5-4	2.5	Monoaxial	0.04	0.24	2000

Table 2: Specifications of MUSA and PEARL at 1064nm, CL51 and CS135. All the instruments are operated in the zenith pointing mode. RFOV indicates again the half-angle rectangular field of view of the instruments.

Instrument	Wavelength (nm)	Pulse Energy (µJ)	Repetition Rate (kHz)	Configuration	Laser Divergence (mrad)	RFOV (mrad)	Approx. Full Overlap Height (m)
MUSA	1064	5.5×10^5	0.02	Biaxial	0.3	0.5	400
PEARL	1064	10^6	0.05	Monoaxial	0.125	0.5	550
CL51	910±10nm	3	6.5	Advanced single-lens optics	0.15 x 0.25	0.56	230 (90 % overlap)
CS135	912±5nm	4.8	10	Single split-lens biaxial	0.35	0.75	300–400

605

Atmospheric
Measurement
Techniques
Discussions
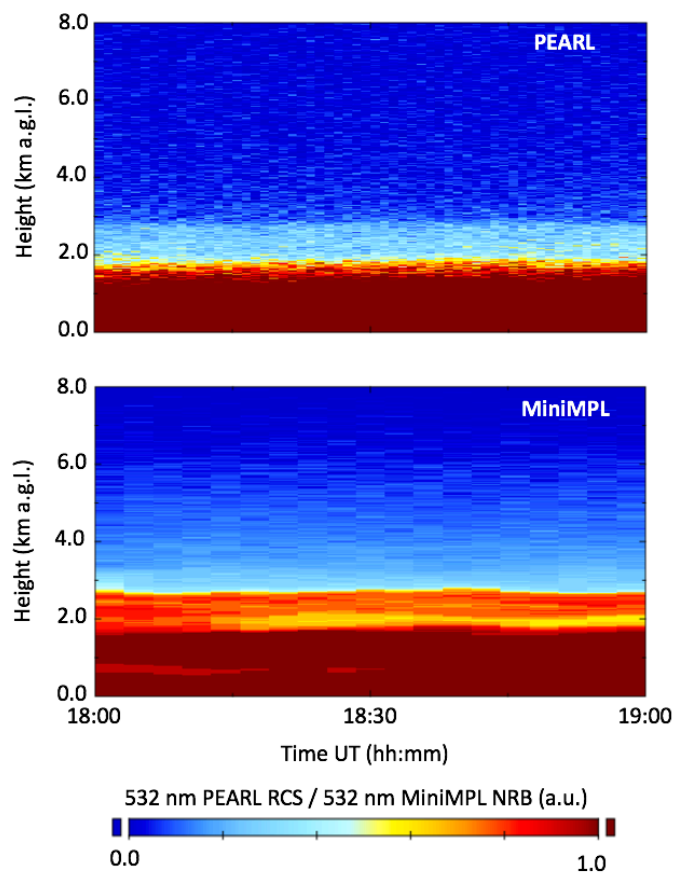
Figure 1: Time series of 532 nm PEARL RCS (top) and MiniMPL NRB (bottom) for the measurements collected on 13 October 2016 from 18:00 to 19:00 UT; heights are above ground level (a.g.l.); raw time and vertical resolutions are 1 minute and 15 m for PEARL, and 5 minutes and 30 m for MiniMPL.

610

Atmospheric
Measurement
Techniques
Discussions
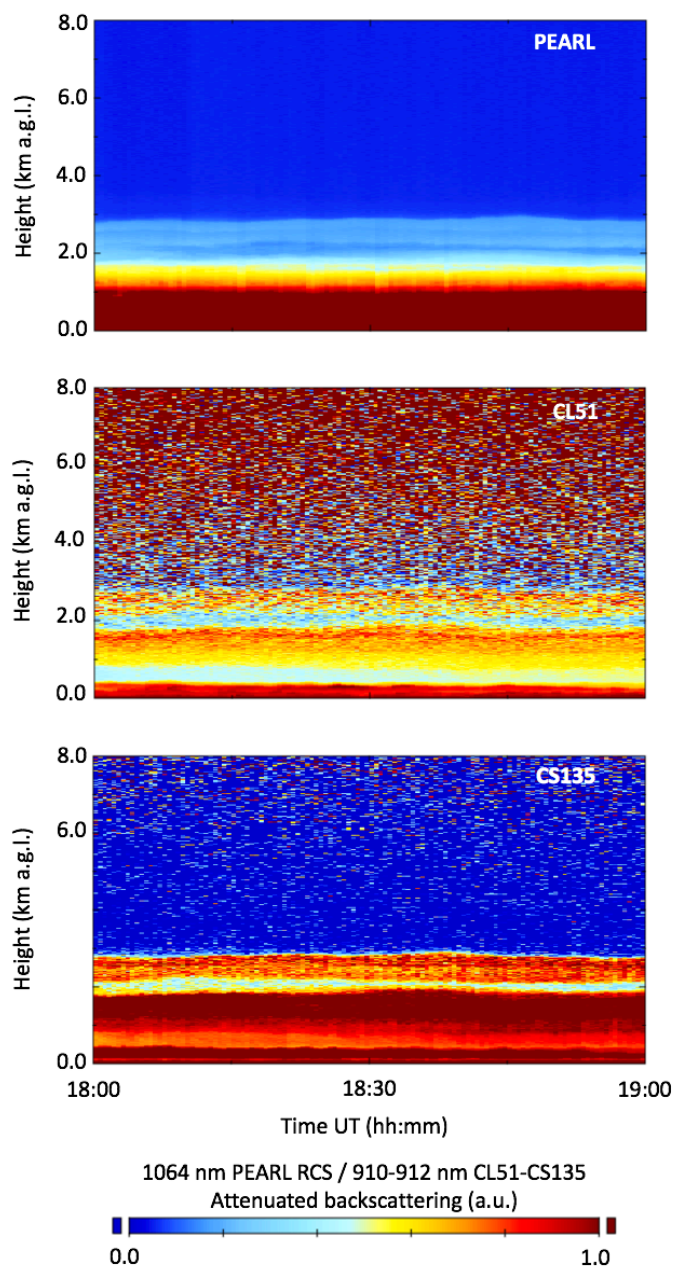
Figure 2: Time series of 1064 nm PEARL Range-Corrected Signal (top) and 905-910 nm CL51/CS135 backscatter profiles (middle/bottom) as provided by the manufacturer software for the measurements collected on 13 October 2016 from 18:00 to 19:00 UT; heights are above ground level (a.g.l.); raw time and vertical resolutions are 1 minute and 7.5 m for PEARL, 30 seconds and 10 m for CL51 and 30 seconds and 5 m for CS135.
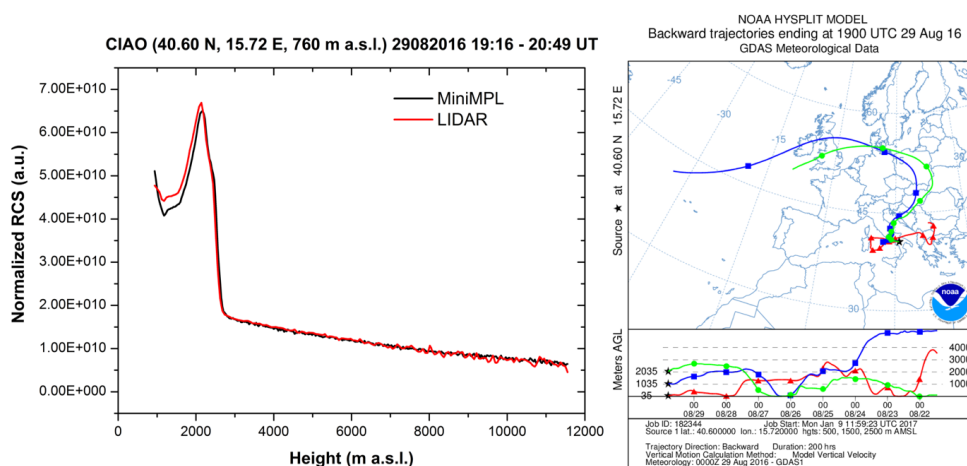
Figure 3: Left panel, comparison between range corrected signals (RCS) obtained from MUSA and MiniMPL on 29 August 2016 from 19:16 to 20:47 UT. Right panel, the corresponding air mass back trajectory analysis performed using NOAA HYSPLIT model started at the three levels from the ground the top layer observed by MUSA and MiniMPL lidars.
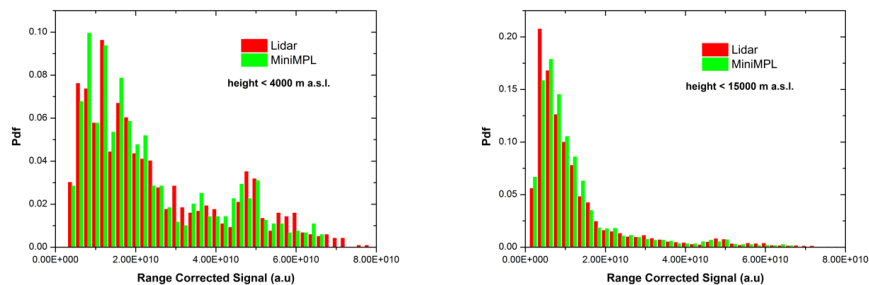
Atmospheric
Measurement
Techniques
Discussions
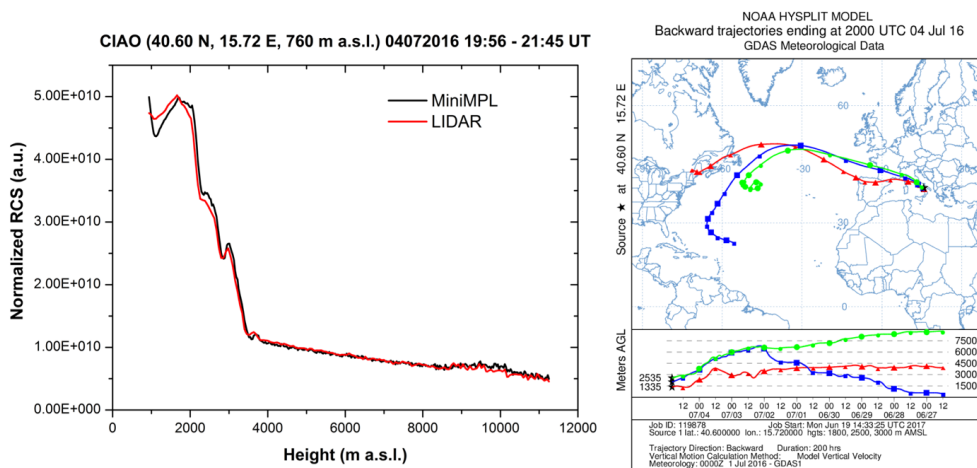
645 **Figure 4**: Left panel, comparison between range corrected signals (RCS) obtained from MUSA and mini-MPL on 04 July 2016 from 19:56 to 21:45 UT; right panel, the corresponding air mass back trajectory analysis performed using NOAA HYSPLIT model started at the three levels from the ground the top layer observed by MUSA and MiniMPL lidars.

650

655
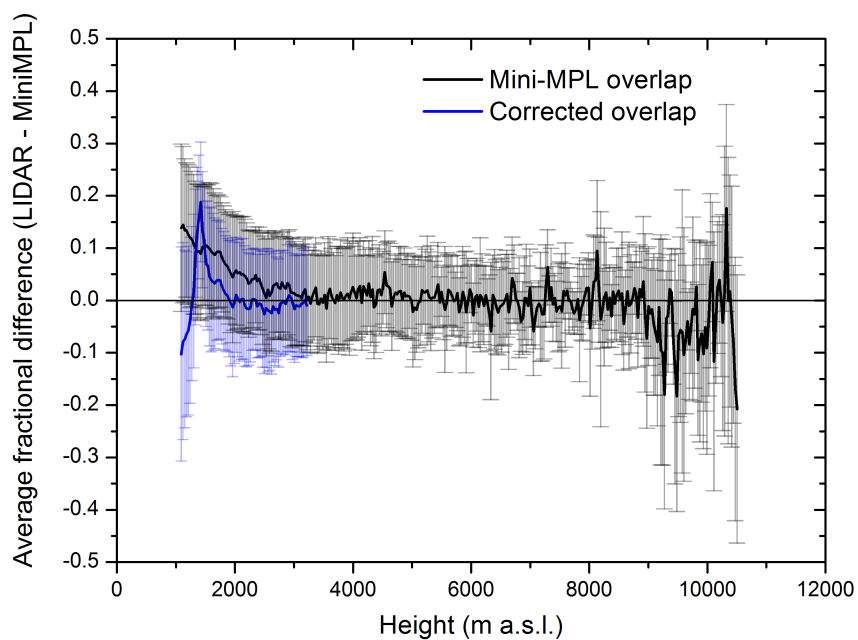
Figure 5: Black line, profiles of the average fractional difference between MUSA and MiniMPL values of RCS calculated on 12 cases of simultaneous and collocated measurements. Blue line, same as black line but applying an additional overlap correction factor to the MiniMPL data processing estimated using the ratio between MUSA and MiniMPL profiles during the cleanest simultaneous measurement session available during INTERACT-II. The vertical bars are the standard deviations of average fractional differences.

680   Figure 6: Pdfs of the RCS values measured by MUSA and MiniMPL below 4 km and along the whole observed atmospheric column.

685

690

695

700

705

710

715

720

Atmospheric
Measurement
Techniques
Discussions
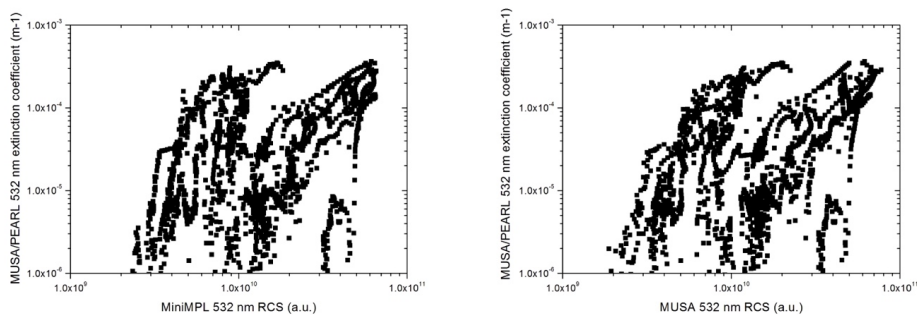
725

Figure 7: Comparison of the scatterplots showing the relationship between MUSA/PEARL 532 nm extinction coefficient and MiniMPL (left panel) and MUSA/PEARL 532 nm RCS (right panel), respectively.
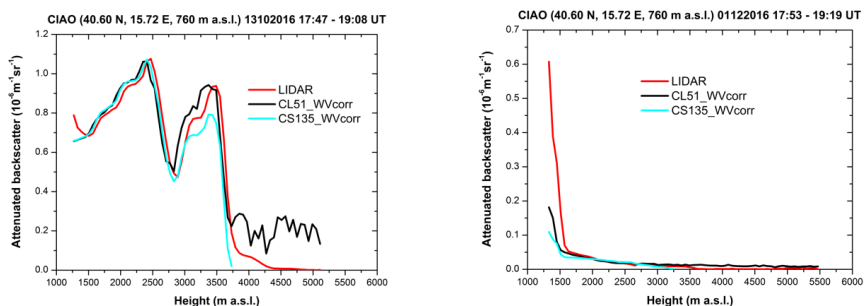
730

735

740

745

750

755

760

Atmospheric
Measurement
Techniques
Discussions

Figure 8. Left panel, comparison between the attenuated backscatter retrieved from MUSA/PEARL, CL51 and CS135 on 13 October 2016 in the time interval from 17:47 to 19:08 UT, using to normalization ranges (below 3 km and above 8 km); right panel, same as left panel but for the 01 December 2016 in the time interval from 17:53 to 19:19 UT. All the ceilometer profiles are corrected for the water vapor absorption affecting the signal extinction at 910-912 nm.
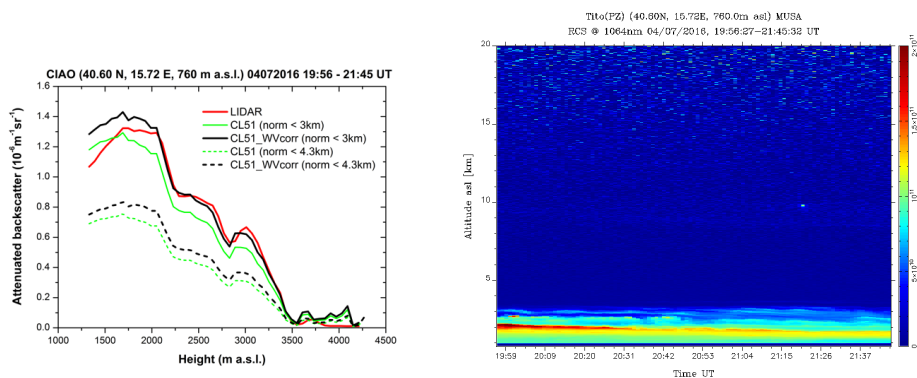
765

770

775

780

785

790

Atmospheric
Measurement
Techniques
Open Access
Discussions
EGU

Figure 9: Left panel, comparison between the attenuated backscatter retrieved from MUSA/PEARL and CL51 on 4 July 2016 from 19:56 to 21:45 UT, using two different normalization ranges (the first below 3 km and the second below 4.3 km); both the raw calibrated profiles and the water vapor calibrated corrected profiles are shown; right panel MUSA/PEARL 1064 nm RCS during the same time.

Atmospheric
Measurement
Techniques
Discussions
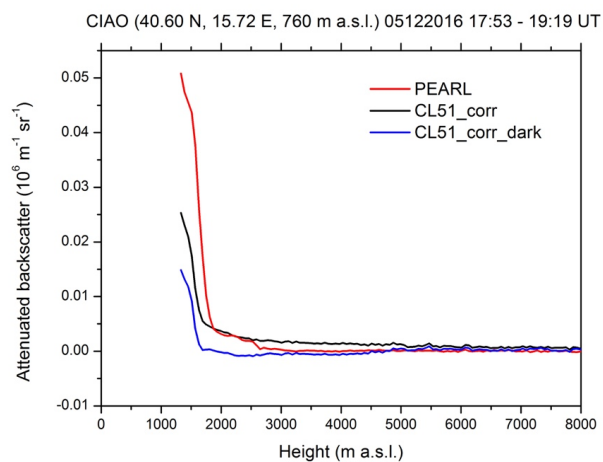

Figure 10: Comparison among the attenuated backscatter profile retrieved from PEARL (red), from CL51 accounting for the water vapour absorption at its operating wavelength (dark) and from CL51 subtracting the dark currents measured separately and then accounting for the water vapour absorption (blue) on 1 December 2016 in the time interval from 17:53 to 19:19 UT.

Atmospheric
Measurement
Techniques
Open Access

Discussions

EGU
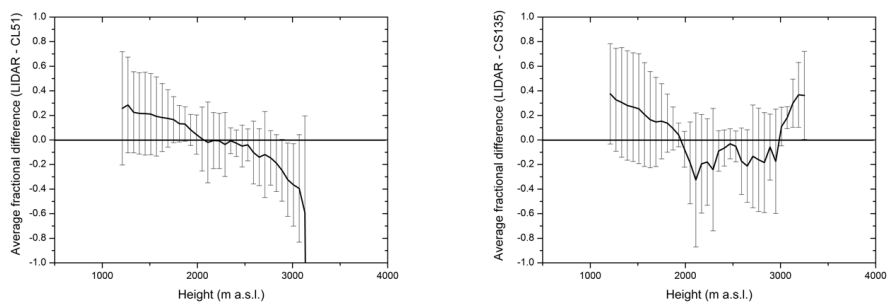
Figure 11: Left panel, profiles of the average fractional difference between MUSA/PEARL and CL51 values of the attenuated
backscatter calculated on 19 cases of simultaneous and collocated measurements; right panel, same as left panel but for
MUSA/PEARL and CS135 calculated on 9 cases. The vertical bars are the standard deviations of average fractional differences.
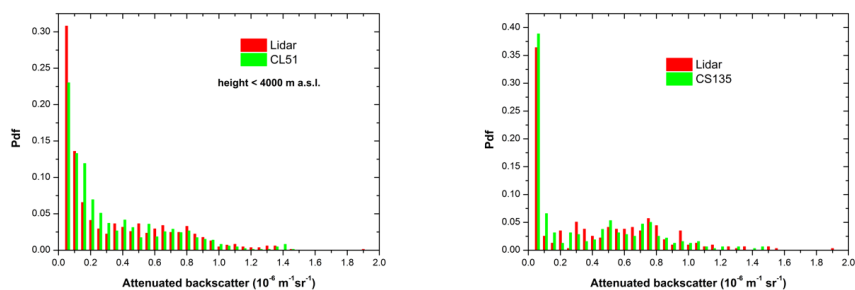
840

845

850

855

860

865

870

875   Figure 12: Pdfs of the attenuated backscatter values measured or estimated by MUSA and CL51 (left panel) and by MUSA and CS135 (right panel) below 4 km and along the whole observed atmospheric column.

880

885

890

Atmospheric
Measurement
Techniques
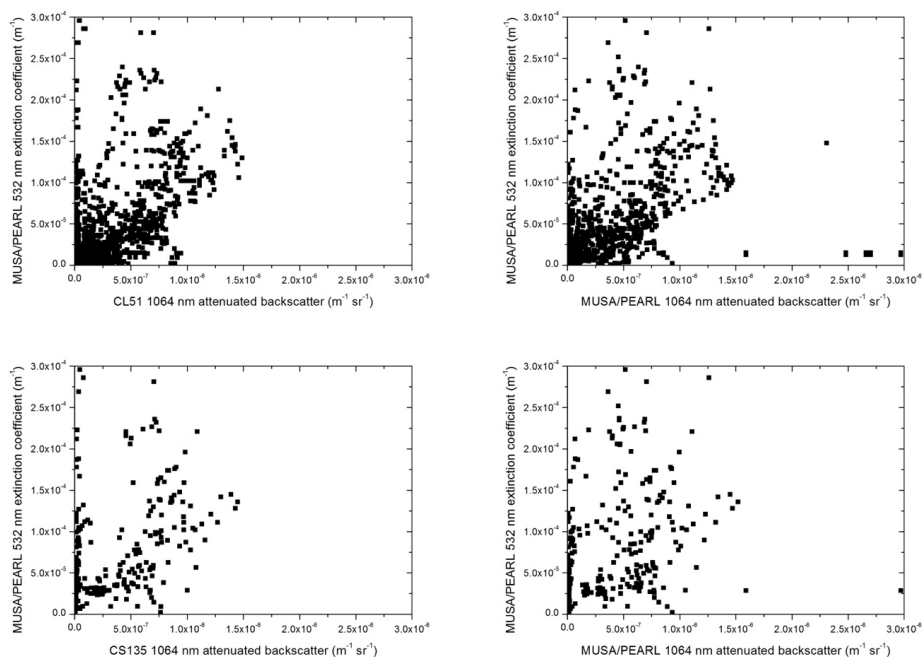Open Access

Discussions

EGU

895

Figure 13: Comparison of the scatterplots showing the 532 nm aerosol extinction coefficient vs 1064 nm attenuated backscatter relationship for CL51 (left top panel) and MUSA/PEARL (right top panel), and for CS135 (left bottom panel) and MUSA/PEARL (right bottom panel), respectively.

900

905

910

Atmospheric
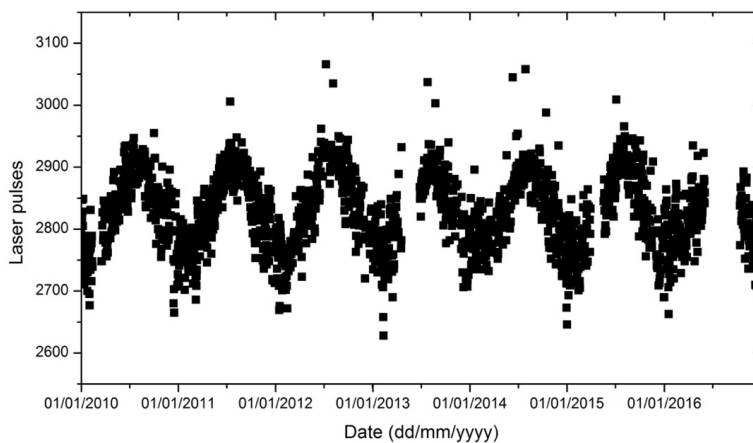Measurement
Techniques
Discussions

Open Access

Figure 14: CHM15k laser pulses per measurement cycle (30 s) as a function of the time for the measurement period from 2010 through 2016.

915